Sun et al. Nanoscale Research Letters (2016) 11:310
DOI 10.1186/s11671-016-1505-7

Nanoscale Research Letters

NANO EXPRESS Open Access

Rear-Sided Passivation by SiN_x:H Dielectric Layer for Improved Si/PEDOT:PSS Hybrid Heterojunction Solar Cells

Yiling Sun[1,2], Pingqi Gao[2], Jian He[2], Suqiong Zhou[2], Zhiqin Ying[2], Xi Yang[2], Yong Xiang[1*] and Jichun Ye[2*]

Abstract

Silicon/organic hybrid solar cells have recently attracted great attention because they combine the advantages of silicon (Si) and the organic cells. In this study, we added a patterned passivation layer of silicon nitride (SiN_x:H) onto the rear surface of the Si substrate in a Si/poly(3,4-ethylenedioxythiophene):poly(styrenesulfonate) (PEDOT:PSS) hybrid solar cell, enabling an improvement of 0.6 % in the power conversion efficiency (PCE). The addition of the SiN_x:H layer boosted the open circuit voltage (V_{oc}) from 0.523 to 0.557 V, suggesting the well-passivation property of the patterned SiN_x:H thin layer that was created by plasma-enhanced chemical vapor deposition and lithography processes. The passivation properties that stemmed from front PEDOT:PSS, rear-SiN_x:H, front PEDOT:PSS/rear-SiN_x:H, etc. are thoroughly investigated, in consideration of the process-related variations.

Keywords: Si/PEDOT:PSS, Hybrid solar cells, SiN_x:H passivation, Photolithography

Background

Over the past several decades, crystalline silicon (c-Si) solar cells have dominated the commercial solar cell market due to multiple factors, such as high power conversion efficiency (PCE) [1], abundance of raw materials, free of toxicological issues, and well-established processing techniques. However, this type of solar cells suffers from drawbacks such expensive processing and large material consumption due to high-temperature treatment and thick substrate required. In recent years, organic photovoltaics emerge as a promising technology in the solar energy field, thanks to simple processing and low material consumption [2–4]. The development of organic solar cells is faced by a grand challenge: the PCE is relatively low due to the low electron–hole separation efficiency. The emergence of c-Si/organic hybrid photovoltaics offers a possible route to low-cost and high-efficiency solar cells by combining the advantages of c-Si and organic materials [5–7]. Recently, poly(3,4ethylenedioxythiophene)/poly (styrenesulfonate) (PEDOT:PSS) has stimulated intense interest in the research community because of its advantageous properties with respect to light transmission and hole conductivity. Up to now, the PCE of PEDOT:PSS hybrid solar cells has been improved to above 13 % [8–10] as a result of efforts in several areas including interface modification [11, 12], surface texturing on Si [13–17], and property tuning of PEDOT:PSS [18]. Typical improvements related to the rear side is to add an ultra-thin interfacial layer of LiF [19], LiQ [9], or $CsCO_3$ [20] between the c-Si layer and the back electrode, with the aims to reduce contact resistance and enhance the rear electric field. With this design, the short circuit current density (J_{sc}) and open circuit voltage (V_{oc}) are both enhanced. However, it is critical to precisely control the thickness of these kinds of layers at a certain value, in order to achieve a satisfied contact resistance while not hindering charge carrier collection.

For the purpose of passivating the n-type c-Si, hydrogenated silicon nitride (SiN_x:H) is an ideal candidate material. SiN_x:H [21], conventionally deposited by plasma-enhanced chemical vapor deposition (PECVD), is known to be widely used in the Si-based solar cell processing. This dielectric layer contains considerable amount of hydrogen bonds and positive charges (typically several 10^{12} cm^{-2}) [22], offering good chemical and

* Correspondence: xiang@uestc.edu.cn; jichun.ye@nimte.ac.cn
[1]School of Energy Science and Engineering, University of Electronic Science and Technology of China, Chengdu 611731, People's Republic of China
[2]Ningbo Institute of Materials Technology and Engineering, Chinese Academy of Sciences, Ningbo 315201, People's Republic of China

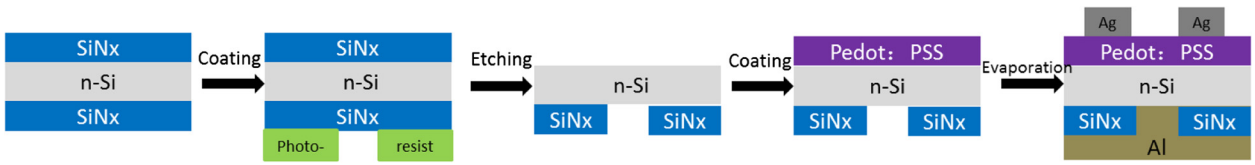

Fig. 1 Process flow of the fabrication of Si/PEDOT:PSS hybrid solar cell with a patterned SiN_x:H passivation layer

field-effect passivation on H-terminated n-type emitter [23]. To date, surface recombination velocities (S_{eff}) below 10 cm/s have been achieved though PECVD method [22, 24].

In this study, we fabricated a hybrid c-Si/organic solar cell with an added passivation layer of PECVD-SiN_x:H at the rear side and investigated its characteristics. First, the PECVD-SiN_x:H layer was thoroughly characterized by surface recombination velocity, focusing on its relations to some aspects including thickness and chemical bond. Second, photoresist was served to protect the SiN_x layer, and chemical etching with diluted hydrofluoric acid (HF) was used to obtain a partial passivation layer with a SiN_x-to-substrate ratio of 60 %. After that, a PEDOT:PSS film was formed on the front side of the substrate by spin-coating, followed by the formation of grid-Ag/full-Al contact layers on the front and rear sides by thermal evaporation. A comparison of the SiN_x:H-passivated device and control sample showed perceivable increases in both J_{sc} and V_{oc}, improving the PCE by 0.6 to 9.0 % under the simulated solar illumination (AM 1.5, 100 mW/cm^2).

Methods

A Si wafer (n-type, single-side polished, float zone, 20 × 20 mm, 300 ± 15 μm in thickness, resistance 3-5 Ωcm) underwent standard RCA (Radio Corporation of American) [25] cleaning and 8 % (volume ratio) HF cleaning. Then, a SiN_x:H passivation layer was deposited upon the double sides of the Si substrate from the gas mixture of SiH_4 (5 sccm), NH_3 (40 sccm), and Ar (40 sccm) for 10 min at a temperature of 350 °C with a pressure of 70 Pa. The prepared films have a thickness of about 100 nm that was measured with a scanning electron microscope (SEM).

A layer of negative photoresist was coated on the SiN_x:H layer by spin-coating at a speed of 3000 rpm for 30 s. Then, the masked Si/SiN_x:H layer was exposed in the UV for 90 s. The exposed portion of the negative photoresist was then washed away using a developer, and the surface underwent an etching process in 0.25 % HF solution for 30 s, removing the portion of the SiN_x:H layer without the protection of photoresist. After washing away the remained photoresist by acetone, a Si substrate partially covered by a SiN_x film was obtained.

Next, the front side of the sample was spin-coated with PEDOT:PSS solution at a speed of 3000 rpm for 1 min, and then heated on the on a hotplate at 130 °C for 10 min to remove the solvents. Finally, a 150-nm-thick grid Ag layer and a 200-nm-thick Al layer were thermal-evaporated on the front side and rear side of the sample, respectively. The fabrication processes of the Si/PEDOT:PSS hybrid solar cell with a patterned SiN_x:H passivation layer was schematically shown in Fig. 1.

The surface topography and thickness of the patterned SiN_x:H passivation layer were observed by SEM (Hitachi S-4800 SEM). The chemical bonding characteristics of the SiN_x:H layers were obtained by attenuated total reflectance Fourier transform infrared spectroscopy

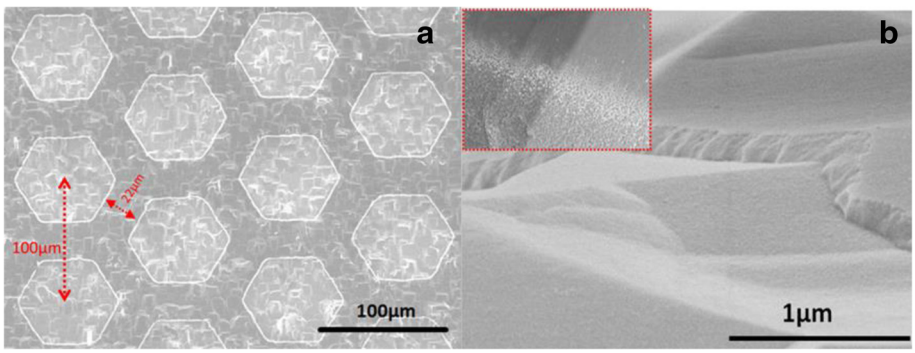

Fig. 2 SEM images of the passivation layer. **a** is the top view. The hexagons are SiN_x patterns, with a center-to-center distance of 100 μm and a spacing of 22 μm. **b** represents SiN_x film with a good etching result and uniform coverage, without residual photoresist and symptom of overetching. The *inset* shows the pores as a result of HF horizontal etching.

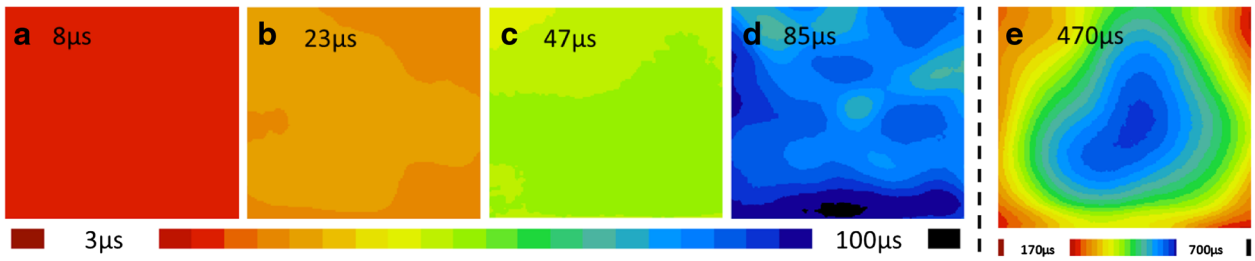

Fig. 3 The mapping of minority carrier lifetime for the Si substrates without passivation (**a**), with coating of front PEDOT:PSS (**b**), with coating of patterned SiN_x:H at the rear side only (**c**), with coating of PEDOT:PSS at the front and patterned SiN_x:H at the rear (**d**), with coating of double-sided SiN_x:H in full area (**e**), respectively. The average lifetime was indicated in each mapping images

(ATR-FTIR, Harrick) and X-ray photoelectron spectroscopy (XPS, AXIS Ultra DLD). Using a microwave photoconductance decay (μ-PCD) technique (WT2000PVN, Semilab), the minority carrier lifetimes of the SiN_x:H layers were characterized. After calibrating the irradiation intensity of the standard silicon photovoltaic device (Oriel, model 91150 V), the current density–voltage (J–V) characteristics of the hybrid solar cells were tested with a Keithley 2400 digital source meter (Keithley) under simulated sunlight (100 mW/cm^2) illumination provided by a xenon lamp (Oriel) with an AM 1.5 filter. The open area of the cells was 0.7 cm × 0.8 cm with 0.11 cm^2 area shaded by the grid of Ag electrodes. Newport silicon detector and 300-W xenon light source with a spot size of 1 × 3 mm was used to measure the external quantum efficiency (EQE).

Results and Discussion

SiN_x:H Surface Topography

The SiN_x:H was finally patterned into many hexagons, with a center-to-center distance between adjacent hexagons of 100 μm and minimum spacing between hexagons of 22 μm. Through this design, we obtained passivation patterns with a passivation-to-substrate coverage ratio of 60 %. Figure 2a shows the patterns after HF etching (0.25 %, 30 s) and ultrasonic cleaning with acetone, where the unpolished Si surface was covered by a uniform layer of hexagonal SiN_x:H. The HF etching (0.25 %, 30 s) produced a steep SiN_x:H edge without residual photoresist or a symptom of overetching (Fig. 2b). It was observed that during the etching process, excessively high concentration of HF or extra etching time could result in pore-like configuration on the SiN_x:H (Fig. 2 add-on). This is because the HF penetrated into the interface between photoresist and SiN_x and horizontal overetching occurred. Apart from creating pores, horizontal overetching could also bring negative impact on or even neutralize the passivation. It was observed that performing etching using HF with a concentration of 0.25 % for 30 s produced optimal passivation and the micron-scale channels between the hexagons could offer enough depth to width ratio for thermal-evaporating electrode materials.

Passivation of the SiN_x:H Layer

The minority carrier lifetime depends on the recombination on the surface and inside of the bulk, as expressed in Eq. 1.

$$\frac{1}{\tau_m} = \frac{1}{\tau_b} + \frac{2S_{\text{eff}}}{W} \tag{1}$$

where τ_m is the measured lifetime, τ_b is the bulk carrier lifetime, S_{eff} is the surface recombination velocity, and W is the wafer thickness. The minority carrier lifetime of

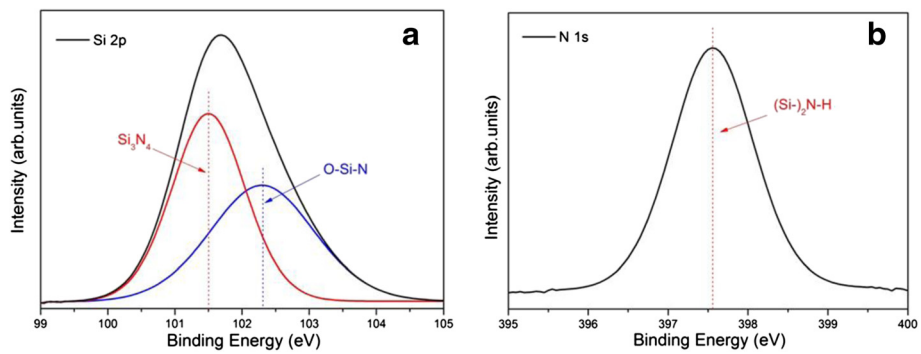

Fig. 4 The Photoemission (XPS) spectra for (**a**) Si 2p and (**b**) N 1s of the SiN_x:H film

Si wafers with different surface treatments was mapped and shown in Fig. 3. The average carrier lifetime increased to 470 μs after the deposition of a 100-nm SiN_x:H layer, in comparison to 7 μs that was measured in the reference of a 300-μm-thick raw FZ-Si wafer (Fig. 3a). Assume that τ_b is infinite in comparison with τ_m, and S_{eff} can be calculated as low as 30 cm/s using Eq. 1. Unfortunately, the HF etching process via opening on the SiN_x:H layer will cause a dramatic reduction in the lifetime of the minority carriers, i.e., from 470 to 47 μs (Fig. 3c). This figure is only 10 % of that of the fully coated sample with SiN_x:H, but still about seven times of that of the reference sample without any passivation (Fig. 3a). To further study the impact of passivation properties both from the front PEDOT:PSS and rear SiN_x:H layer, the patterned sample and the reference sample were spin-coated with a PEDOT:PSS film on the top surface. The comparison revealed that the average lifetime of the minority carrier of the sample solely coated by PEDOT:PSS was 23 μs (Fig. 3b), while the one of the sample with both PEDOT:PSS and patterned SiN_x:H was 85 μs (Fig. 3d). Inferred from this improvement in carrier lifetime, an implied increase of 0.020 V in V_{oc} and 1 % in PCE are both expected.

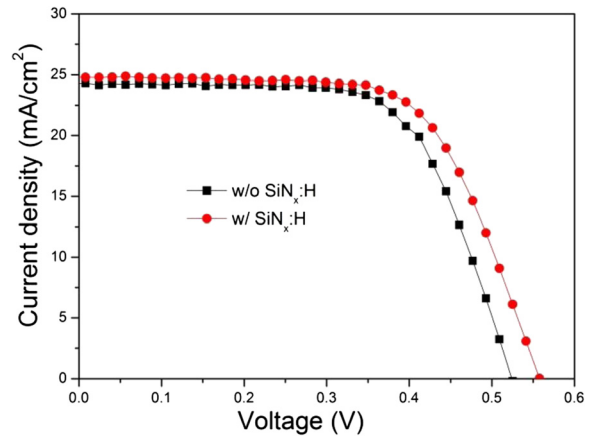

Fig. 6 Current–voltage curves of Si/PEDOT:PSS devices with or without a passivation layer of patterned SiN_x:H

Chemical Bond Structure of the SiN_x:H Layer

XPS and FTIR were used to confirm the chemical bond characteristics of the SiN_x:H film. Figure 4 shows the XPS spectra of the SiN_x:H film, with all binding energy values being calibrated to the contaminant carbon peak at 284.8 eV. XPS spectrum indicates that the Si/N molar ratio is 40:29. The peak of Si 2p spectra was located around 102 eV (Fig. 4a), composed of the Si 2p signal of the Si_3N_4 group at 101.5 eV [26] and the signal of O–Si–N group at 102.3 eV [27]. There exists an oxygen element in the SiN_x:H film, that is because the sample had adsorbed oxygen or H_2O in the air. Figure 4b shows that N 1s peak consists of a single symmetric peak at 397.6 eV. According to an earlier work by Shallenberger et al. [28], the peak located at 397.6 eV is most likely related to a specific bonding style $(Si–)_2N–H$ i.e., one N atom is bonded to two Si atoms and one H atom. Meanwhile, no other N 1s peaks like $(Si–)_2N–O$ at 399.7 eV, $Si–N(–O)_2$ at 402.8 eV, and $NO_3–$ at 407 eV were found in the spectrum. Therefore, the impact of the absorbed water molecules is excluded and Si–N and Si–Si–N bonds are

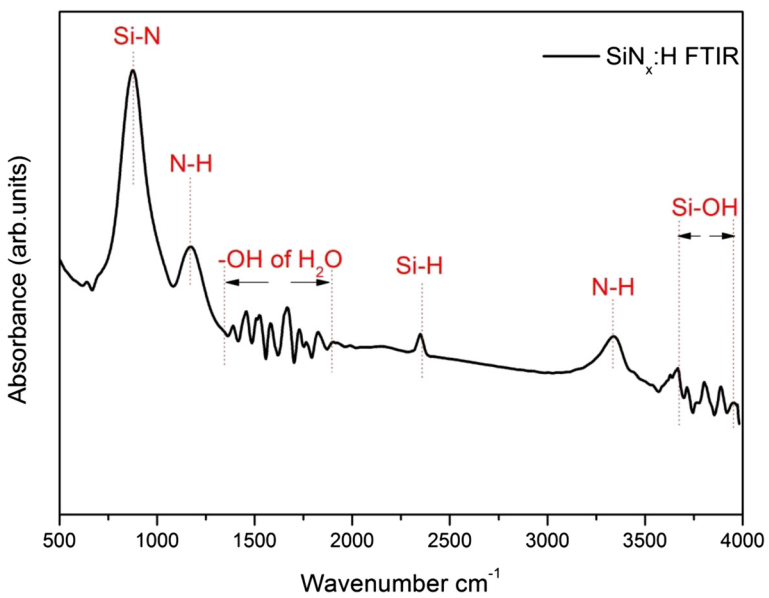

Fig. 5 ATR-FTIR curve of SiN_x:H film

Table 1 Photovoltaic characteristics of Si/PEDOT:PSS heterojunction device with or without a SiN_x:H layer

	V_{oc} (V)	J_{sc} (mA/cm^2)	FF (%)	PCE (%)	R_s (Ωcm^2)	Rsh (Ωcm^2)
W/O SiN_x:H	0.523 ± 0.011	24.0 ± 0.18	67.78 ± 0.27	8.40 ± 0.21	7.95 ± 0.42	2570.80 ± 5.78
W/ SiN_x:H	0.557 ± 0.014	24.8 ± 0.22	65.24 ± 0.22	9.02 ± 0.15	10.39 ± 0.40	5544.18 ± 4.69

Note: Values were obtained by averaging five devices with a calculated confidence interval of 95 %

most likely the dominant bonding types in the passivation film, which will contribute mainly to the field-effect passivation.

ATR-FTIR analysis was carried out in order to obtain details on the chemical state of the SiN_x:H film. ATR-FTIR absorption curves in Fig. 5 show a dominant absorption feature around 878 cm^{-1} which can be ascribed to the Si–N bending stretching vibration [29]. According to earlier ATR-FTIR analyses reported by Patil et al., the peak around 2349 cm^{-1} occurring in the ATR-FTIR spectrum resulted from the vibration of Si–H bond [30]. The N–H absorption bond at the 1173 and 3340 cm^{-1} are typically ascribed to the SiN_x:H film [31, 32]. In addition, the peaks in the region from 3580 to 3670 cm^{-1} and around 1650 cm^{-1} peaks can be explained by the absorption of the H_2O molecules on the surface of the SiN_x:H film [33]. The above analysis on the chemical bond structure shows good agreement with the analysis by XPS, indicating that Si–N bond is the dominant bond type in the SiN_x:H film. What is more, hydrogen-related bonds such as N–H and Si–H were observed in ATR-FTIR spectrum, which may offer good chemical passivation on H-terminated n-type Si.

Photovoltaic Characteristics of the Solar Cells

To verify the effect of the patterned passivation layer at the rear side, we fabricated a few heterojunction solar cells with/without a SiN_x:H layer. Figure 6 shows the current density–voltage (J–V) characteristics of the related Si/PEDOT:PSS hybrid solar cells. Table 1 lists the average values of J_{sc}, V_{oc}, fill factor (FF), and PCE of the fabricated devices. The passivation effect of the SiN_x:H layer on the rear surface is directly reflected in the measured value of V_{oc} of the Si /PEDOT:PSS solar cell. The V_{oc} of the SiN_x:H layer coated samples increased by 0.033 V in comparison with the samples without a passivation layer, reaching a maximum of 0.557 V. This can be attributed to the decrease of the charge carrier recombination that occurred on the rear surface. The little bit increase in J_{sc} (from 24.0 to 24.8 mA/cm^2), possibly because of the enhanced capability of carriers collection at a longer wavelength range. The series resistance (R_s) reached an acceptable value of 10.39 Ωcm^2 for the SiN_x:H-coated hybrid cells which is comparable to the R_s of 7.95 Ωcm^2 for the reference sample. It is reasonable for the little bit increase in R_s because of the reduced contact area between the Si and the rear electrodes. Similarly, a little degradation in FF was also observed. For the above reasons, the addition of the SiN_x:H layer did not bring significant changes to the PCE of the SiN_x:H-coated solar cells, with a PCE of 9.0 % and only 0.6 % higher than the reference sample. Better results can be expected if more efforts are made to optimize the coverage percentage and the contact properties of the rear side.

The EQE was measured, as shown in Fig. 7. Cells with the SiN_x:H layers displayed a higher EQE value in the visible and near-infrared region in comparison with the

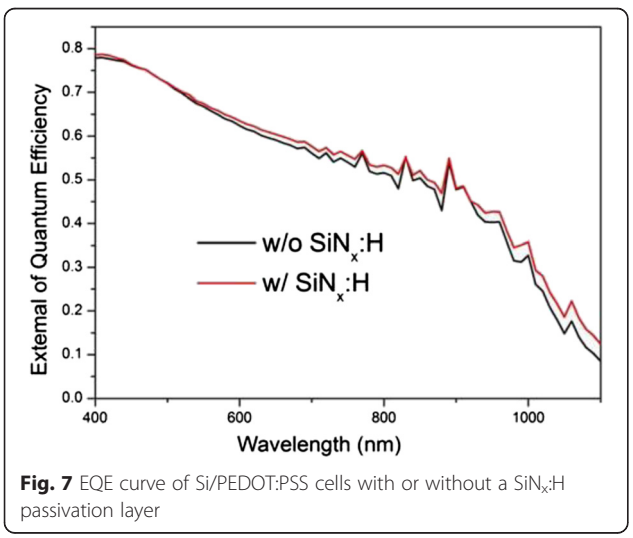

Fig. 7 EQE curve of Si/PEDOT:PSS cells with or without a SiN_x:H passivation layer

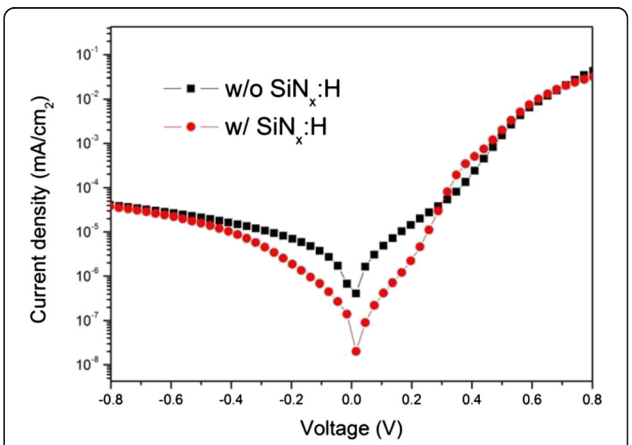

Fig. 8 Dark J–V curve of Si/PEDOT:PSS devices with or without SiN_x:H passivation layer

Table 2 Diode ideality factors (n), reverse saturation current densities (J_s), and Schottky barrier heights (Φ_{bi}) values of Si/PEDOT:PSS heterojunction solar cells with or without a SiN_x:H layer

	J_s (A/cm^2)	Diode ideality factors (n)	Φ_{bi} (eV)
W/o SiNX:H	1.08×10^{-6}	2.59	0.77084
W/ SiNX:H	5.55×10^{-7}	2.45	0.78794

reference cells, which is consistent with the increase of J_{sc}, benefiting from recombination suppression occurring on the rear surface.

In order to further investigate the performance of the cells with the SiN_x:H passivation layer, the dark J–V characteristics were measured and the results were plotted in Fig. 8. It was observed that saturation current density (J_s) reduced significantly after the addition of the SiN_x:H layer on the rear layer. The typical rectifying characteristic curve indicated that SiN_x:H-coated hybrid cells exhibited better behaviors characteristic of heterojunction as well as a diode. The dark J–V curves were simulated according to the thermionic emission model as follows:

$$J = J_s\left[\exp\left(\frac{eV}{nkT}\right) - 1\right] \tag{2}$$

$$J_s = A^* A T^2 \exp\left(-\frac{\Phi_{bi}}{KT}\right) \tag{3}$$

where J_s is the reverse saturation current density value, V is the applied voltage, T is the absolute temperature (298 K), k is the Boltzmann constant (1.38×1023 m^2 kg s^{-2}K^{-1}), q is the electronic charge (1.6×10^{-19}C), A is the contact area, A^* is the effective Richardson constant (about 252 A cm^{-2} K^{-2} for n-type Si), and Φ_{bi} is the barrier height of Schottky diode. From the dark J–V curves under the forward bias condition (Fig. 8) and Eqs. 2 and 3, the n, J_s, and Φ_{bi} of the heterojunction solar cells were extracted, as listed in Table 2. The device with the SiN_x:H layers displayed a J_s value of 5.55×10^{-7}A/cm^2, approximately a half of that of the cells without the SiN_x:H layer (which was 1.08×10^{-6}A/cm^2). Here, the diode ideality factor n in this Schottky diode is linked to the quality of the p–n junction which is influenced by the recombination velocity on the rear surface of Si. The SiN_x:H-coated device has a smaller n value of 2.45, which implied that lower density of the defect centers in the space charge region due to the better passivation quality of the SiN_x:H. And the Φ_{bi} value was also increased about 0.02 eV from 0.77 eV in the reference solar cell to 0.79 eV for the SiN_x:H-coated cell.

Conclusions

In summary, we have demonstrated that the performance of Si/PEDOT:PSS hybrid solar cells can be improved by adding a patterned passivation layer of SiN_x:H onto the rear surface of the Si substrate. A PCE of 9 % was achieved for the SiN_x:H-coated solar cells. Compared to the cells without rear passivation, a 0.6 % improvement in PCE was obtained. As the shrink of contact areas would increase the R_s value, further optimizations on the pattern configurations and the contact between Si and Al are needed to achieve more higher PCE for Si/PEDOT:PSS hybrid cells.

Abbreviations

AFM, atomic force microscopy; ATR-FTIR, attenuated total reflectance Fourier transform infrared spectroscopy; J_{sc}, photocurrent density; PCE, power conversion efficiency; PEDOT:PSS, poly(3, 4-ethylenedioxythiophene): poly(styrenesulfonate); V_{oc}, open circuit voltage; XPS, X-ray photoelectron spectroscopy

Competing Interests

The authors declare that they have no competing interest.

Authors' contributions

YS, PG carried out the design and drafted the manuscript. JH, SZ, ZY, and XY commented on the results and revised the manuscript. YX and JY conceived the design and supervised the research. All authors read and approved the final manuscript.

Acknowledgements

This work is supported by the Zhejiang Provincial Natural Science Foundation (No. LY14F040005, LR16F040002), the National Natural Science Foundation of China (Grant No. 61404144, 51472044), the International S&T Cooperation Program of Ningbo (Grant No. 2015D10021), and the "Thousand Young Talents Program" of China, One Hundred Person Project of the Chinese Academy of Sciences, the Instrument Developing Project of the Chinese Academy of Sciences (No. yz201328).

Received: 24 February 2016 Accepted: 30 May 2016
Published online: 28 June 2016

References

1. Moldovan A, Feldmann F, Zimmer M, Rentsch J, Benick J, Hermle M (2015) Tunnel oxide passivated carrier-selective contacts based on ultra-thin SiO2 layers. Sol Energ Mat Sol C 142:123–127
2. Mei J, Ogawa K, Kim YG, Heston NC, Arenas DJ, Nasrollahi Z, McCarley TD, Tanner DB, Reynolds JR, Schanze KS (2009) Low-band-gap platinum acetylide polymers as active materials for organic solar cells. ACS Appl Mater Interfaces 1:150–161
3. Zhao G, He Y, Li Y (2010) 6.5 % efficiency of polymer solar cells based on poly(3-hexylthiophene) and indene-C(60) bisadduct by device optimization. Adv Mater 22:4355–4358
4. Hoth C, Schilinsky P, Choulis S, Brabec C (2008) Printing highly efficient organic solar cells. Nano letters 8:2806–2813
5. He L, Jiang C, Wang H, Lai D, Heng Tan Y, Seng Tan C, Rusli (2012) Effects of nanowire texturing on the performance of Si/organic hybrid solar cells fabricated with a 2.2 μm thin-film Si absorber. Appl Phys Lett 100:103104
6. He L, Jiang C, Rusli, Lai D, Wang H (2011) Highly efficient Si-nanorods/organic hybrid core-sheath heterojunction solar cells. Appl Phys Lett 99:021104
7. Wendy U, Janke J, Alivisatos A (2002) Hybrid nanorod-polymer solar cells. Science 295:2425–2427
8. He J, Gao P, Liao M, Yang X, Ying Z, Zhou S, Ye J, Cui Y (2015) Realization of 13.6% efficiency on 20 μm thick Si/organic hybrid heterojunction solar cells via advanced nanotexturing and surface recombination suppression. ACS Nano 9:6522–6531
9. Liu R, Lee ST, Sun B (2014) 13.8% efficiency hybrid Si/organic heterojunction solar cells with MoO3 film as antireflection and inversion induced layer. Adv Mater 26:6007–6012

10. Yu P, Tsai CY, Chang JK, Lai CC, Chen PH, Lai YC, Tsai PT, Li MC, Pan HT, Huang YY, Wu CI, Chueh YL, Chen SW, Du CH, Horng SF, Meng HF (2013) 13 % efficiency hybrid organic/silicon nanowire heterojunction solar cell via interface engineering. ACS Nano 7:10780–10787
11. Sheng J, Fan K, Wang D, Han C, Fang J, Gao P, Ye J (2014) Improvement of the SiOx passivation layer for high-efficiency Si/PEDOT:PSS heterojunction solar cells. ACS Appl Mater Interfaces 6:16027–16034
12. Chi D, Qi B, Wang J, Qu S, Wang Z (2014) High-performance hybrid organic-inorganic solar cell based on planar n-type silicon. Appl Phys Lett 104:193903
13. J. He, Z. Yang, P. Liu, S. Wu, P. Gao, M. Wang, S. Zhou, X. Li, H. Cao, J. Ye, Enhanced electro-optical properties of nanocone/nanopillar dual-structured arrays for ultrathin silicon/organic hybrid solar cell applications, Adv. Energy Mater., DOI: 10.1002/aenm.201501793 (2015)
14. Pudasaini PR, Ruiz-Zepeda F, Sharma M, Elam D, Ponce A, Ayon AA (2013) High efficiency hybrid silicon nanopillar-polymer solar cells. ACS Appl Mater Interfaces 5:9620–9627
15. Uma K, Subramani T, Syu H-J, Lin T-C, Lin C-F (2015) Fabrication of silicon nanowire/poly(3,4-ethylenedioxythiophene):poly(styrenesulfonate)-graphene oxide hybrid solar cells. J Appl Phys 117:105102
16. Ge Z, Xu L, Cao Y, Wu T, Song H, Ma Z, Xu J, Chen K (2015) Substantial improvement of short wavelength response in n-SiNW/PEDOT:PSS solar cell. Nanoscale Res Lett 10:998
17. Wang H, Wang J, Rusli (2015) Hybrid Si nanocones/PEDOT:PSS solar cell. Nanoscale Res Lett 10:191
18. Thomas JP, Srivastava S, Zhao L, Abd-Ellah M, McGillivray D, Kang JS, Rahman MA, Moghimi N, Heinig NF, Leung KT (2015) Reversible structural transformation and enhanced performance of PEDOT:PSS-based hybrid solar cells driven by light intensity. ACS Appl Mater Interfaces 7:7466–7470
19. Zhang Y, Liu R, Lee S-T, Sun B (2014) The role of a LiF layer on the performance of poly(3,4-ethylenedioxythiophene):poly(styrenesulfonate)/Si organic-inorganic hybrid solar cells. Appl Phys Lett 104:083514
20. Zhang Y, Cui W, Zhu Y, Zu F, Liao L, Lee S-T, Sun B (2015) High efficiency hybrid PEDOT:PSS/nanostructured silicon Schottky junction solar cells by doping-free rear contact. Energy Environ Sci 8:297–302
21. Bustarret E, Bensouda M, Habrard M, Bruyère J, Poulin S, Gujrathi S (1988) Configurational statistics in a-SixNyHz alloys: a quantitative bonding analysis. Phys Rev B 38:8171–8184
22. Schmidt J, Aberle AG (1999) Carrier recombination at silicon–silicon nitride interfaces fabricated by plasma-enhanced chemical vapor deposition. J Appl Phys 85:3626
23. Mäckel H, Lüdemann R (2002) Detailed study of the composition of hydrogenated SiN[sub x] layers for high-quality silicon surface passivation. J Appl Phys 92:2602
24. Elmiger JR, Schieck R, Kunst M (1997) Recombination at the silicon nitride/silicon interface. J Vac Sci Technol A 15:2418–2425
25. Kern W, Puotinen DA (1970) Cleaning solutions based on hydrogen peroxide for use in silicon semiconductor technology. Rca Rev 31:187–205
26. Hu M, Gao X, Sun J, Weng L, Zhou F, Liu W (2012) The effects of nanoscaled amorphous Si and SiNx protective layers on the atomic oxygen resistant and tribological properties of Ag film. Appl Surf Sci 258:5683–5688
27. Naskar S, Wolter SD, Bower CA, Stoner BR, Glass JT (2005) Verification of the O–Si–N complex in plasma-enhanced chemical vapor deposition silicon oxynitride films. J Appl Phys 87:261907
28. Shallenberger J, Cole D, Novak S (1999) Characterization of silicon oxynitride thin films by X-ray photoelectron spectroscopy. J Vac Sci Technol A 17:1086–1090
29. Kakiuchi H, Nakahama Y, Ohmi H, Yasutake K, Yoshii K, Mori Y (2005) Investigation of deposition characteristics and properties of high-rate deposited silicon nitride films prepared by atmospheric pressure plasma chemical vapor deposition. Thin Solid Films 479:17–23
30. Patil L, Pandey K, Bange J, Gaikwad S, Gautam D (2005) Effect of deposition temperature on the chemical properties of thermally deposited silicon nitride films. Opt Mater 27:663–670
31. Bustarret E, Bensouda M, Habrard MC, Bruyère JC, Poulin S, Gujrathi SC (1988) Configurational statistics in a-SixNyHz alloys: a quantitative bonding analysis. Phys Rev B 38:8171–8184
32. Pereira M, Diniz J, Doi I, Swart J (2003) Silicon nitride deposited by ECR–CVD at room temperature for LOCOS isolation technology. Appl Surf Sci 212–213:388–392
33. Ay F, Aydinli A (2004) Comparative investigation of hydrogen bonding in silicon based PECVD grown dielectrics for optical waveguides. Opt Mater 26:33–46